Nano World Journal

https://doi.org/10.17756/nwj.2023-s3-165

Research Article

Open Access

Optical Transparency Classification in Polyethylene Based Nanocomposite Films Using Deep Neural Networks

Vitthal Sadashiv Gutte[1*], Shrihari Mahadeo Bondar[2], Yogesh R Kulkarni[1], Shounak Suave[1], Balaso Nivrutti Jagdale[1] and Nilima Zade[3]

[1]Department of Computer Engineering and Technology, Dr. Vishwanath Karad MIT World Peace University , Pune, India

[2]Department of Mechanical Engineering, Dr. Vishwanath Karad MIT World Peace University, Pune, India

[3]Department of Computer Science and Engineering, Symbiosis Institute of Technology (Pune Campus), Symbiosis International (Deemed University), Pune, Maharastra, India

[*]Correspondence to:
Vitthal Sadashiv Gutte,
Department of Computer Engineering and Technology,
Dr. Vishwanath Karad MIT World Peace University,
Pune, India.
E-mail: nilima.zade@gmail.com

Received: July 31, 2023
Accepted: November 01, 2023
Published: November 03, 2023

Citation: Gutte VS, Bondar SM, Kulkarni YR, Suave S, Jagdale BN, et al. 2023. Optical Transparency Classification in Polyethylene Based Nanocomposite Films Using Deep Neural Networks. *NanoWorld J* 9(S3): S930-S936.

Published by United Scientific Group

Abstract

Applications of deep learning techniques in nanotechnology are particularly important since they allow for the optimal design of multi-characteristic nanomaterials. To differentiate between films composed of PS latex particles and multi walled carbon nanotubes (MWCNTs) in terms of their light-transmission characteristics connected deep neural network (DNN) classifiers was fully trained. Intensity of transmitted light, particle size of PS latexes, percentage of MWCNT nanofillers by mass, and annealing temperature all played roles in classifying the spectroscopic data. Experiments were run to find the optimum values for the DNN classifier's hyperparameters using a custom Bayesian optimizer. Proposed DNN classifiers may be evaluated using a variety of different measures, such as accuracy, the confusion matrix, cross-entropy loss, F1-score, recall, precision, and area under the curve calculated from receiver operating properties curvatures. When using sigmoid functions in the hidden layer units and setting the layer sizes to 30 and 20, respectively, the best results are shown on both the training and testing data sets for accuracy, precision, recall, and F1-score. Experimental data is few, but computational studies show that DNNs may be used to categorize the optical transparency of film samples.

Keywords

Polyethylene, Bayesian optimization, Machine learning, Nanocomposites, Optical transparency

Introduction

The engineering sector has been faced with the difficult and expensive challenge of designing polyethylene nanocomposites with numerous characteristics. Optimizing the desired measurement response during the production of such multifunctional materials might require many time-driven experiments [1]. Here, the ideal measurement response may be gracefully tuned using a combination of experimental and software-based techniques like machine learning, paving the way for the conservation of time, energy, and materials. As a result, machine learning has lately shown great promise as an auxiliary tool, allowing substantial progress to be achieved in the optimum design of polyethylene nanocomposites through the provision of accurate predictions in the modelling of a large array of technical factors [2]. Researchers have employed machine learning to simulate the microstructure of energy-storage nanocomposites and forecast their tensile strength after carbon nanotube (CNT) infusion. In materials science, DNNs and other recent machine learning approaches may be effectively employed as classifiers, despite their more common usage as regression-based models

for predicting a broad variety of attributes of such complex materials [3].

Technical challenges encountered during the synthesis of chemical compounds and material characterization have slowed the experimental progress toward the best design for transparent, electrically conductive nanocomposite films [4]. Costly nanofillers are used to alter the film's shape and HDPE characteristics, and this has a major effect on the samples' conductivity and transparency responses. The optical transparency of insulating polyethylene is reduced when excessive concentrations of CNTs are included into the polyethylene itself, as in polystyrene (PS) latex particles [5]. Determining the correct concentration of CNTs is crucial for maintaining the film's multifunctionality, but this may involve a few time-consuming, trial-and-error trials. Researchers have been able to improve the computational design of such multi-characteristic nanomaterials by utilizing previous measurement data sets found in scientific archives. With the use of artificial intelligence models like DNNs, the output characteristics of nanocomposite films may be estimated or categorized without the need for laborious and time-consuming testing [6, 7].

To show the value of DNNs for polyethylene nanocomposites, we evaluate the performance of several models that use predictors like the mean diameter of particle size latex particles, the mass fraction of, the annealing temperature, and the transparency of the film to categorize the optical transparency of multiwall-loaded particle size latex films into three opacity classes. Using a Bayesian optimizer and careful hyper-parameter tuning, researchers have developed DNN classifiers with the highest accuracy attainable. Each DNN model's classification performance was measured using standard error measurements, a confusion matrix, and ROC plots. The classification abilities of the DNNs were further explored by calculating the area under the curve (AUC) for each class.

A subset of machine learning algorithms called DNNs takes its cues from the brain's structure [8]. Such machines are analogous to ANNs, but with additional levels of complexity, in the context of deep learning. DNNs may assume many different topological shapes, such as multilayer perceptron's (MLP), convolutional neural networks (CNN), or recurrent neural networks (RNN), depending on the order in which their layers are applied [9, 10]. Instead, fully-connected MLP-based DNNs will be the key research focus of this paper. Compared to a standard feed-forward neural network (FFNN), a fully connected DNN(FCDNN) comprises more than two hidden layer units, each of which is adorned with many neurons.

As can be seen in figure 1, a fully linked DNN structure consists of several levels [11]. Neurons are the essential parts of DNNs that do data processing. In DNNs, the neurons in the input layer are the first to receive information represented by A!, A",..., and x#. The weighted interconnection nodes among the input and output layers relay information from the input layer to the intermediate hiding layers. The input neurons that share information in the buried layers are given additional weights that account for network bias. Activation functions (AFs) are used to do a mathematical processing once input is

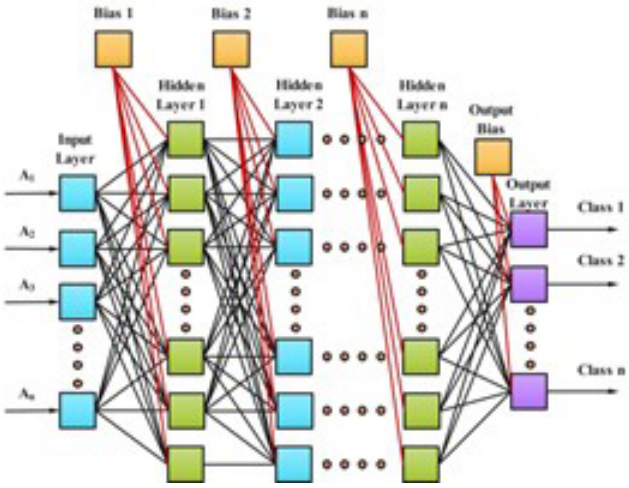

Figure 1: An illustration of an FCDNN classifier with linked neurons arranged in various layers.

received by the buried layer neurons.

The activation of the hidden and output neurons is critically dependent on the AFs. When one hidden neuron is engaged, it feeds the processed data to the hidden neurons below it. This process is repeated until the final output layer is achieved. When a FCDNN classifier employs a SoftMax function in its output layer, it provides a response to the input neurons that may be regarded of as a classification score or a posterior probability. For the posterior probability, both binary and multiclass classification, f(An), for each class is calculated using the subsequent formula [12].

$$f(A_n) = \frac{e^{A_n}}{\sum_{n=1}^{m} e^{A_n}} \quad (1)$$

Where m is the total no of distinct categories in the resulting data. Using the error tolerance established during network topology training, a FCDNN classifier compares the computed classification scores against a target answer. If the network classifier estimates a large enough error among the network output and the target value, it will employ backpropagation to retrain the input predictors. The cross-entropy loss function, by far the most popular during training, may be stated as follows for multiclass classification [13].

$$\text{Cross-entropy loss} = -\frac{1}{N}\sum_{k=1}^{N} y_k \cdot \log(\hat{y}_k) \quad (2)$$

Where

yk desired outcome

y2# expected outcome

N total number of observations

The cross-entropy loss is minimised by gradually decreasing the network's weights and biases throughout training.

Computational Methodology

The experimental data, used software, hyperparameter choice, DNN optimization, and performance measurement techniques are all described in this part.

The DNN classifiers' optical data comes from UV-Visible spectrophotometer measurements of photon transmission through coatings of PS latex/MWCNT nanocomposites. Global network statistics are displayed in table 1.

The full collection of experimental data has been classified as either opaque, semi-transparent, or transparent based on the 1-. values of nanocomposite films. The different classes and their corresponding frequency ranges are summarized in table 2 below.

The relationship between each category and the I-. and C*'+ predictors are shown graphically in figure 2. As can be listed in table 2 and figure 2, there is a large discrepancy between the frequency counts of the various classes in the network data utilized by fully connected DNN classifiers. However, this does not indicate that implementing uneven data would result in disparate predictions when DNN classifiers are adequately adjusted.

Using the "fitcnet" tool in MATLAB, we have constructed DNN models, estimated error metrics, and determined various performance assessment indices. Only 30% (153 out of 512) of the dataset was used for validation, whereas 70% (359) was used for training the network. For DNN applications, the data size may be on the smaller side, but there is no higher data set obtained in this field. Class labels from table 2 were applied to DNN output variables, whereas values from table 1 were used as predictors in the input layer. The training method now uses a Bayesian optimizer as the underlying optimization technique. The well-known limited memory Broyden-Fletcher-Goldfarb-Shanno quasi-Newton method (LBFGS) has been used as a solution all through training when the fitcnet command is added into the compiler script [14-17]. The purpose of the LBFGS technique is to iteratively minimize the cross-entropy loss among the anticipated and target values.

Every single DNN model uses softmax as the AF in the output layer, as was previously described. We have used a trial-and-error strategy to test out various configurations of hidden layers, hidden neuron geometries, and activation functions (AFs) like the ReLU, tanh, sigmoid, and identity

Table 1: Data from the network statistics.

Input variables	Unit	Statistical indices			
		Minimum	Maximum	Mean	Standard deviation
D_{PS}	nm	385	565	495.24	65.89
C_{CNT}	wt.%	0	15	2.87	4.18
T_a	°C	100	260	178	47.15
I_{tr}	(%)	0	84.95	26.94	24.99

Table 2: Class frequency and data limits.

Class	Transmission limits	Frequency of data
Semi-transparent	40% < *I* < 70%	165
Opaque	I_{tr} ≤ 40%	335
Transparent	I_{tr} ≥ 80%	18

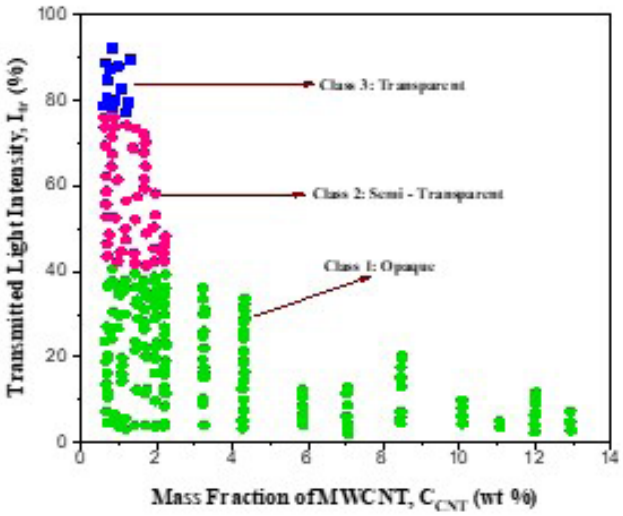

Figure 2: Distributions of each class's frequency count depending on their calculated transmitted light intensity, Itr.

(linear) function to achieve the highest possible classification accuracy across both datasets. A thorough description of the universal error measures used to evaluate the arrangement performances of the five top DNNs classifiers, all of which achieve acceptable accuracy values better than 98%.

Each DNN classifier model's multiclass classification performance was initially evaluated using accurateness, history loss for cross-entropy, and data loss. However, it is possible that the use of only two measures is insufficient in evaluating classifier performance. Because of this, not only the confusion matrix but also precision, recall, and F1-scores were studied [18]. The four basic binary classification metrics must be computed using the confusion matrix that is derived from the target and predicted values. Using these measures, one may describe accuracy as the fraction of all possible variables that are correctly classified as positive or negative.

$$\text{Accuracy} = \frac{TP+TN}{TP+TN+FP+FN} \quad (3)$$

Where,

TP = True positives

FP = False positives

TN = True negatives

FN = False negatives

The percentage of true positives that were correctly detected is the recall, the second statistic. It is equivalent to the TPR or sensitivity.

$$\text{Recall} = \frac{TP}{TP+FN} \quad (4)$$

F1-score was employed as a final statistic in this study. Harmonic mean of recall and accuracy, or F1-score, is stated as follows in equation 5 [19].

$$F1_{Score} = 2 \times \frac{\text{Precision} \times \text{Recall}}{\text{Precision} + \text{Recall}} \quad (5)$$

Another popular statistic for judging a classifier's efficacy is its precision, which is defined as the percentage of positive variables that were properly detected (Equation 6).

$$\text{Precision} = \frac{TP}{TP+FP} \quad (6)$$

These statistical error factors are added to the evaluation of the five DNN classifiers' classification performance using receiver operating characteristic (ROC) curves, which are class-specific. The ability of the DNN classifiers to correctly categorize data is graphically represented by the ROC curve [20]. True positive rate (TPR) and false positive rate (FPR) can be plotted against one another to get the ROC curve (FPR). The area under the curve (AUC) operating characteristic curve for each class provides insight into the discriminatory power of the proposed DNN classifiers. The AUC measures how well a classifier separates two groups of interest [21, 22].

This study consequently plots the ROC curves for each class independently to calculate AUC values and thoroughly explores their respective classification capabilities. The best DNN model was determined by plotting confusion matrices for both the training and validation sets of data.

Results and Discussions

Five completely connected DNN topologies were developed, and their classification skills were statistically assessed. In combination, these topologies may reach precisions more than 98%. Model-specific information on the hiding layer geometry, like the no of hiding layers, the total no of neurons, and the AFs deployed in each hidden layer unit, is provided in table 3.

DNN classifier accuracy and loss values of cross-entropy for experimented and predicted data sets are displayed as bar graphs in figure 3a and 3b. Figure 3a demonstrates that model

Table 3: Specifications on the projected DNN classifiers' topology.

Models	AFs	Hidden layer size
1	[relu, tanh]	2
2	[sigmoid, sigmoid]	2
3	[tanh, tanh]	2
4	[sigmoid, linear]	2
5	[sigmoid, sigmoid, tanh]	3

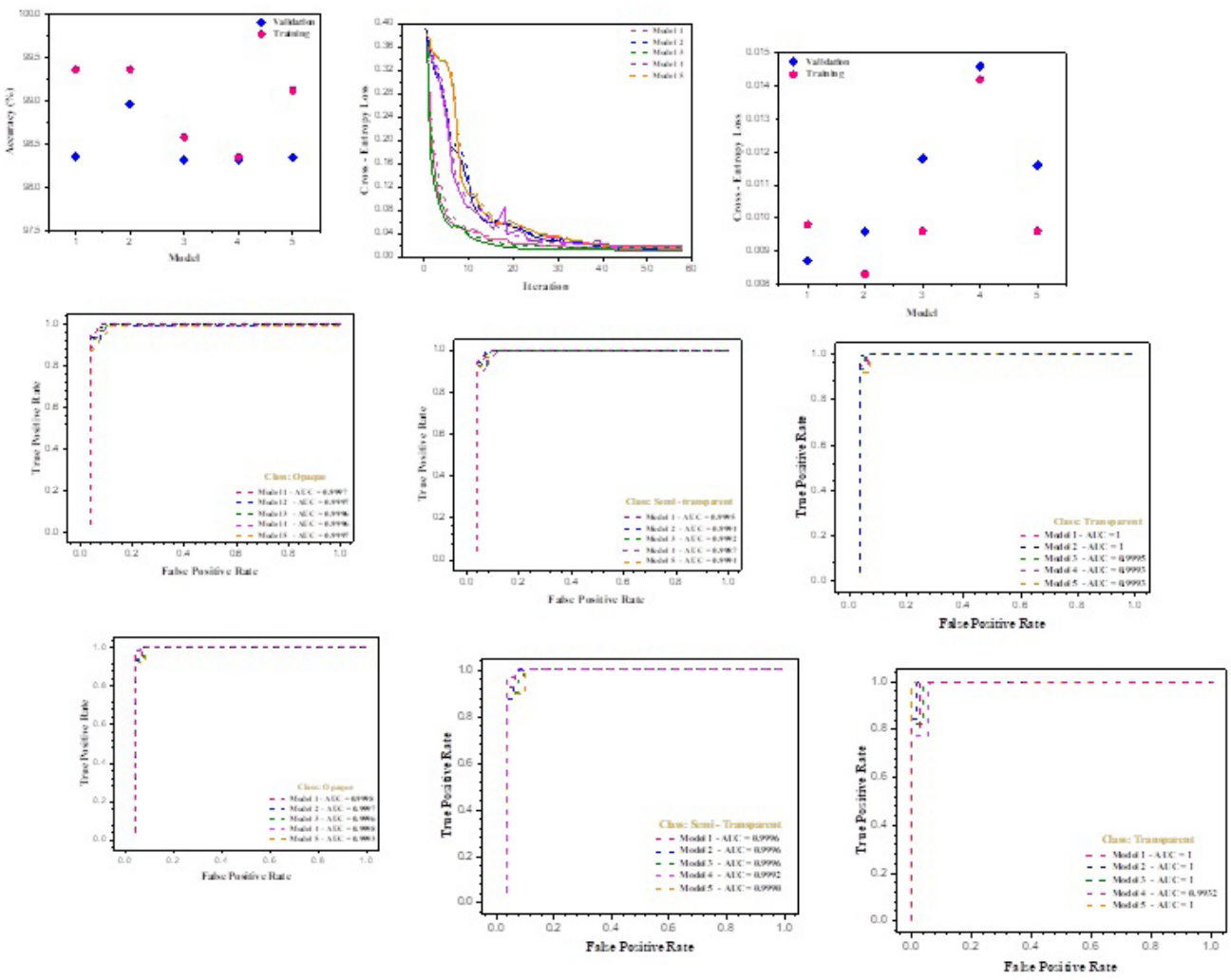

Figure 3: Plots showing **(a)** Accurateness, **(b)** History loss, and **(c)** Cross-entropy loss for every DNN classifier proposal. Each class's ROC curve has been presented for both the experimented **(d–f)** Predicted and **(g–i)** Values.

2 obtained the highest levels of accuracy, with a training data set accuracy of 99.36% and a validation data set accuracy of 98.96%. Conversely, the accuracy of DNN models 1, 3, 4, and 5 was determined to be 99.36%, 98.58%, 98.57%, and 99.12% during training, and 98.13%, 98.32, 98.31, and 98.34% during validation, respectively. These numerical findings show that, compared to other DNN classifiers, model 2 has a significantly greater validation accuracy.

Model 2's training set produced the lowest cross-entropy loss value (0.0083) while model 1's validation set produced the highest (0.0096) value. The calculated values for the cross-entropy loss for models 1, 3, 4, and 5's training and validation data sets, respectively, were 0.0098, 0.0096, 0.01142, and 0.0096. Model 2 has a somewhat larger validation loss compared to model 1. Other error statistical criteria must be examined to overcome this issue and more precisely establish which model has superior categorization ability. All DNN classifier models' stability and believability were analyzed using cross-entropy loss history plots before doing calculations of such error indices. Figure 3c shows a loss history plot. The estimated history plots reveal a progressive drop in both the training and validation losses leading up to the minimal cross-entropy values. In addition, there was no noticeable variation between training and validation losses for any of the DNN classifiers that were deployed. These graphs also illustrate that there is no indication of overfitting, as the curves of the cross-entropy losses flatten after reaching their minimal values.

The AUC values for the ROC curves were produced to further evaluate the classification performance of classifiers on each individual class. Figure 3d to 3i displays the ROC curves that were developed for each class. ROC curves show that models 1 and 2 have the greatest AUC values when compared to other classifiers for both the experimented (Figure 3d, 3e and 3f) and prediction (Figure 3g, 3h and 3i) information processing. Models 1 and 2 are pitted against one another in a battle for the best DNN classifier by comparing their accuracy, cross-entropy, and area under the curve (AUC) values. Bar graphs of recall, F1-score metrics, and precision, for each model are displayed in figure 4a to 4d to help the reader determine which model has superior classification performance. The bar graphs show that the greatest and identical accuracy, recall, and F1-scores were obtained for the experimented models 1 and 2, respectively, at 99.17% and 99.16%, respectively. When compared to the other classifiers, model 2's evaluation metrics

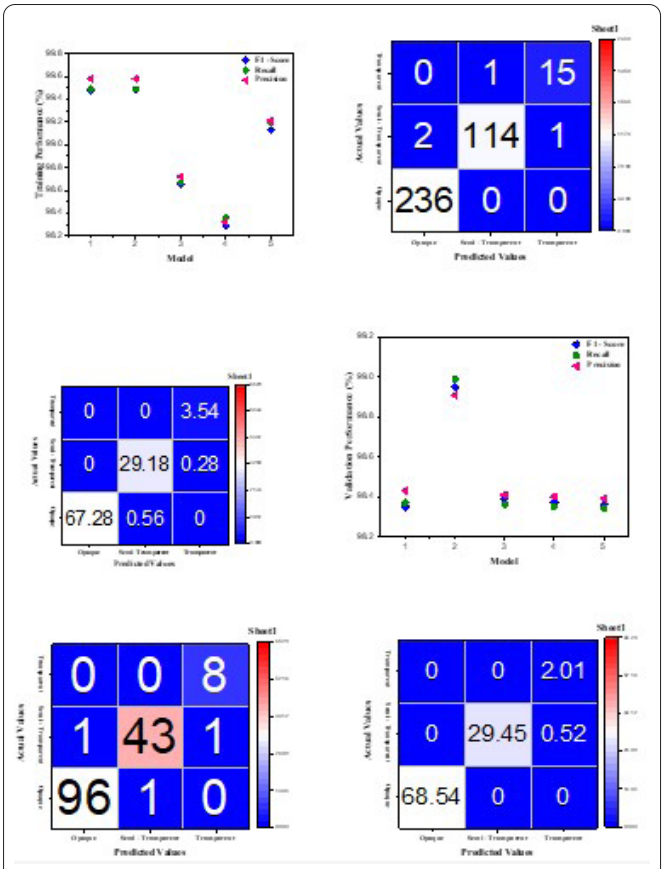

Figure 4: (a) Training and **(b)** Validation precision, recall, and F1-score metrics calculated using various DNN classifiers. Using confusion matrices, we were able to see the distribution of true and false predictions over both the training **(c-d)** validation sets **(e-f)**.

are much higher (98.07% accuracy, 98.06% recall, and 98.02% F1-score), as shown in figure 4d. Based on these findings, model 2 appears to be the most effective MLP-based DNN classifier for distinguishing between opacity levels in PS latex/MWCNT nanocomposite films. Table 4 displays the results of several statistical error metrics computations performed on all created classifiers. These metrics include accurateness, cross entropy loss, precision, recall, and F1-score.

Following a thorough search for the optimal DNN classifier model based on calculated error indices, we used a confusion matrix to visually assess the classification accuracy of each class. A common tool for solving classification issues is the confusion matrix, which summarizes the outcomes of a

Table 4: DNN classification evaluation metric computations.

Error metrics	Model number (Training)					Model number (Validation)				
	1	2a	3	4	5	1	2a	3	4	5
Accuracy	0.9916	0.9916	0.9833	0.9805	0.9889	0.9803	0.9869	0.9804	0.9803	0.9803
C-entropy	0.0084	0.0071	0.0087	0.0129	0.0089	0.0079	0.0087	0.0104	0.0134	0.0109
Precision	0.9917	0.9917	0.9833	0.9805	0.9889	0.9807	0.9870	0.9806	0.9807	0.9807
Recall	0.9916	0.9916	0.9833	0.9805	0.9889	0.9804	0.9869	0.9804	0.9804	0.9804
F1-score	0.9916	0.9916	0.9832	0.9805	0.9888	0.9801	0.9866	0.9804	0.9801	0.9801

Note: a = Best fully connected DNN classifier.

classifier's predictions and makes it easy to compare them to the target values. Using a confusion matrix, how many guesses were made for each class and how many were right were examined. Heat maps (percentage-based representations) of confusion matrices are displayed in figure 4b and 4c and figure 4e and 4f, respectively, when the best DNN classifier, model 2, is applied to experimented and predicted values.

Both the experimented and predicted values had successful opaque film predictions as shown by the calculated results in figure 4b to 4e. There were only two and one incorrectly predicted semi-transparent samples in the training set (n = 113) and validation set (n=49), respectively. Similarly, in those data sets when 12 and 5 transparent samples were used, respectively, just 1 sample was incorrectly labelled. The percentages of properly recognized samples in the training data and the percentages calculated for the testing data for each class were similarly very consistent (Figure 4c and 4f). The improved prediction accuracy of model 2 was also validated by computational findings based on percentages.

Conclusion

This is the first study to compare the efficacy of five different fully connected DNN classifiers for determining how transparent various nanocomposite films. Five best models with accuracies greater than 98% were selected after extensive testing of different hidden layer shapes and AFs. For the best DNN classifier, we found that utilizing sigmoid AFs in the hidden layers of a model with 30 and 20 hidden neurons yielded the highest classification performance. It has better accuracy, F1-score, recall, and precision than other DNN classifiers on the validation data set. It was shown using confusion matrices that just one or two variables in each of two categories (semi-transparent and transparent) were misclassified (333 opaque, 162 semitransparent and 17 transparent out of 512). Computational results from this study suggest that an optimized network may effectively classify the optical transparency or opacity of nanocomposite films from a small, asymmetric raw data set. To better build nanocomposite films with the appropriate optical features, take advantage of our fully linked DNN classifiers to forecast their coatings' optical characteristics.

Acknowledgements

None.

Conflict of Interest

None.

References

1. Prasanth IS, Jeevanandam P, Selvaraju P, Sathish K, Ahammad SKH, et al. 2023. Study of friction and wear behavior of graphene-reinforced AA7075 nanocomposites by machine learning. *J Nanomater* 2023: 1-5. https://doi.org/10.1155/2023/5723730
2. Kumar DD, Balamurugan A, Suresh KC, Kumar RS, Jayanthi N, et al. 2023. Study of microstructure and wear resistance of AA5052/B4C nanocomposites as a function of volume fraction reinforcement to particle size ratio by ANN. *J Chem* 2023: 1-12. https://doi.org/10.1155/2023/2554098
3. Girimurugan R, Selvaraju P, Jeevanandam P, Vadivukarassi M, Subhashini S, et al. 2023. Application of deep learning to the prediction of solar irradiance through missing data. *Int J Photoenergy* 2023: 1-17. https://doi.org/10.1155/2023/4717110
4. Möller B, Pirklbauer J, Klingner M, Kasten P, Etzkorn M, et al. 2023. A super-resolution training paradigm based on low-resolution data only to surpass the technical limits of STEM and STM microscopy. In Proceedings of the IEEE/CVF Conference on Computer Vision and Pattern Recognition, PP 4262-4271.
5. Alexey G, Klyachin V, Eldar K, Driaba A. 2020. Autonomous Mobile Robot with AI based on Jetson Nano. In Proceedings of the Future Technologies Conference (FTC) 2020, pp 190-204.
6. Chen CH. 2007. Signal and image processing for remote sensing. CRC/Taylor & Francis.
7. Wang Y, Jiang H, Hamamoto K. 2022. Space-mode compressor by using nano-pixel. *Japn J Appl Phys* 61: SK1022. https://doi.org/10.35848/1347-4065/ac7b0e
8. Wang J, Bai J, Huang X, Zhou X, Zhao L, et al. 2019. Transparent object sensing with enhanced prior from deep convolutional neural network. In Artificial Intelligence and Machine Learning in Defense Applications 11169: 145-152.
9. Satishkumar P, Mahesh G, Meenakshi R, Vijayan SN. 2021. Tribological characteristics of powder metallurgy processed Cu-WC/SiC metal matrix composites. *Mater Today Proc* 37: 459-465. https://doi.org/10.1016/j.matpr.2020.05.449
10. Elsheikh AH, Shanmugan S, Muthuramalingam T, Thakur AK, Essa FA, et al. 2022. A comprehensive review on residual stresses in turning. *Adv Manuf* 1-26. https://doi.org/10.1007/s40436-021-00371-0
11. Satyanarayana G, Narayana KL, Rao BN. 2021. Incorporation of Taguchi approach with CFD simulations on laser welding of spacer grid fuel rod assembly. *Mater Sci Eng* 269: 115182. https://doi.org/10.1016/j.mseb.2021.115182
12. Satishkumar P, Krishnan GG, Seenivasan S, Rajarathnam P. 2023. A study on tribological evaluation of hybrid aluminium metal matrix for thermal application. *Mater Today Proc* 81: 1097-1104. https://doi.org/10.1016/j.matpr.2021.04.389
13. Meng K, Jiang B, Youcef-Toumi K. 2021. Neural network assisted multi-parameter global sensitivity analysis for nanostructure scatterometry. *Appl Surf Sci* 570: 151219. https://doi.org/10.1016/j.apsusc.2021.151219
14. Satishkumar P, Rakesh AI, Meenakshi R, Murthi CS. 2021. Characterization, mechanical and wear properties of Al6061/Sicp/fly ashp composites by stir casting technique. *Mater Today Proc* 37: 2687-2694. https://doi.org/10.1016/j.matpr.2020.08.530
15. Dharmaiah G, Sridhar W, Balamurugan KS, Chandra Kala K. 2022. Hall and ion slip impact on magneto-titanium alloy nanoliquid with diffusion thermo and radiation absorption. *Int J Ambient Energy* 43(1): 3507-3517. https://doi.org/10.1080/01430750.2020.1831597
16. Liu S, Tu X, Xu C, Chen L, Lin S, et al. 2021. An optimized deep neural network for overhead contact system recognition from LiDAR point clouds. *Remote Sens* 13(20): 4110. https://doi.org/10.3390/rs13204110
17. Chen M, Han J, Liu J, Zheng F, Geng S, et al. 2023. Output prediction of helical microfiber temperature sensors in cycling measurement by deep learning. *Photonic Sens* 13(3): 230308. https://doi.org/10.1007/s13320-023-0681-1
18. Chen Y, Ding Z, Wang J, Zhou J, Zhang M. 2022. Prediction of metasurface spectral response based on a deep neural network. *Opt Lett* 47(19): 5092-5095. https://doi.org/10.1364/OL.468277
19. Abushanab WS, Moustafa EB, Harish M, Shanmugan S, Elsheikh AH. 2022. Experimental investigation on surface characteristics of Ti6Al4V alloy during abrasive water jet machining process. *Alex Eng J* 61(10): 7529-7539. https://doi.org/10.1016/j.aej.2022.01.004

20. Ortega-Piwonka I, Hejda M, Alanis J, Lourenço J, Hurtado A, et al. 2022. Spike propagation in a nanolaser-based optoelectronic neuron. *Opt Mater Exp* 12(7): 2679-2696. https://doi.org/10.1364/OME.451706

21. Lee SH. 2021. Astigmatism-based displacement sensor powered by deep neural networks. *Sens Actuators A Phys* 327: 112763. https://doi.org/10.1016/j.sna.2021.112763

22. Hao Y, Liu Y, Wu T, Li J, Sun Y, et al. 2022. Improved bidirectional networks for nanostructure color design. *Opt Commun* 520: 128419. https://doi.org/10.1016/j.optcom.2022.128419